



# Fabrication and processing of bacterial cellulose/silver nanowire composites as transparent, conductive, and flexible films for optoelectronic applications

Denisha Gounden<sup>1</sup>  | Michael N. Pillay<sup>1</sup>  | Vashen Moodley<sup>1</sup>  |  
Nolwazi Nombona<sup>2</sup>  | Werner E. van Zyl<sup>1</sup> 

<sup>1</sup>School of Chemistry & Physics,  
University of KwaZulu-Natal (Westville  
Campus), Durban, South Africa

<sup>2</sup>Department of Chemistry, University of  
Pretoria, Pretoria, South Africa

## Correspondence

Werner E. van Zyl, School of Chemistry &  
Physics, University of KwaZulu-Natal  
(Westville Campus), Private Bag X54001,  
Durban 4000, South Africa.  
Email: [vanzylw@ukzn.ac.za](mailto:vanzylw@ukzn.ac.za)

## Funding information

National Research Foundation  
South Africa, Grant/Award Number:  
108424; University of KwaZulu-Natal  
(UKZN)

## Abstract

This work reports on the engineering and fabrication of transparent, conductive, and flexible films made as a composite of bacterial cellulose microfibrils (BMF), a polymer (either PVA or PEO), and silver nanowires (AgNWs) as viable and cost-effective replacements to commercial indium-tin oxide (ITO) and fluorine-doped tin oxide (FTO) transparent conductors. The studies conducted indicate that the optical and mechanical properties of BMF-polymer substrates are tuneable by varying the ratio of BMF to polymer. An optimized ratio of 70:30 of BMF to polymer was established for BMF-PVA and BMF-PEO composites. The optimized composite films were coated with varying amounts of AgNWs. As the AgNW loading increased, the deposition density of AgNW networks increased, while the sheet resistance and optical transmittance decreased. The optimum AgNW loading was determined at 0.20 mg for both composite films. The BMF-PVA-AgNW film displayed transmittance between 81% and 71% and an average resistivity of  $9.462 \pm 0.588 \Omega/\text{sq}$  while the BMF-PEO-AgNW films showed transmittance between 73% and 65% and an average resistivity of  $9.388 \pm 0.1375 \Omega/\text{sq}$ . These properties compared well to that of commercial ITO and FTO glass substrates. The findings promote cellulose-based composites as low-cost, lightweight, and durable substrates for optoelectronic applications.

## KEYWORDS

bacterial cellulose, conductive, optoelectronics, poly(vinylalcohol), silver nanowires, transparent

## 1 | INTRODUCTION

Transparent electronics is an evolving technology that replaces traditional opaque semiconductor materials with transparent materials.<sup>1</sup> Efficient, transparent

conductors (TCs) should compromise between sufficient transparency within the visible spectral region and moderate electrical conductivity, as they are neither 100% optically transparent nor metallically conductive,<sup>2</sup> in theory, TCs are thus considered a contradictory

This is an open access article under the terms of the [Creative Commons Attribution-NonCommercial](https://creativecommons.org/licenses/by-nc/4.0/) License, which permits use, distribution and reproduction in any medium, provided the original work is properly cited and is not used for commercial purposes.

© 2023 The Authors. *Journal of Applied Polymer Science* published by Wiley Periodicals LLC.

combination when assessing their electronic bands. Transparent materials are often classed as insulators, but in contrast to conductor and semiconductor materials, the energy gap between the valence and conduction band of an insulator is large. Transparent organic conductors such as poly(3,4-ethylenedioxythiophene) (PEDOT) and poly(3,4-ethylenedioxythiophene): poly(styrene sulfonate) PEDOT:PSS are examples of materials that can bridge the gap between transparency and conductivity.<sup>3,4</sup>

Metal oxide TCs such as ITO currently dominate the thin-film photovoltaic (PV) market as electrode materials due to their superior conductivity and high transparency.<sup>5</sup> Despite its excellent transparency and conductivity, this metal oxide is expensive, scarce, brittle, and requires costly deposition techniques, often onto rigid substrates.<sup>6,7</sup> These expenses and intrinsic properties prevent ITO from being amenable to low-cost, roll-to-roll manufacturing, and applicability toward flexible PV devices.<sup>8,9</sup> A feasible alternative to common metal oxide and polymer TCs is cellulose materials that can be fabricated into transparent and flexible films.<sup>10</sup> As one of the most ubiquitous and abundant polymers on Earth, cellulose is cheaper and more sustainable than its metal oxide counterparts and exhibits properties such as low thermal expansion and mechanical flexibility.<sup>11,12</sup> Cellulose can be extracted and isolated from various sources, including algae, tunicate, trees, and bacteria.<sup>13</sup> Although cellulose is the primary structural component of most plants, it is also secreted by certain aerobic bacteria, most often from the *Acetobacter* genera, via a biotechnological mechanism originating from carbon sources.<sup>14</sup> Bacterial cellulose (BC) is biosynthesized into a polymer by assembling D-glucose monomers only and has greater purity and crystallinity.<sup>15,16</sup> Although these properties highlight cellulose as a potential replacement to conventional TC substrates or use in other optoelectronic applications, one drawback of cellulose is its non-conductive nature.

It has been widely demonstrated that conductivity can be achieved by coating materials with metallic nanoparticles such as gold (Au), silver (Ag), or platinum (Pt).<sup>17–21</sup> Studies commonly use Ag as reports have shown that it is the most conductive and cheapest among these metals. The conductivity of metallic nano-spheres is reportedly low as their small size results in numerous inter-particle junctions.<sup>22</sup> Unlike nano-spheres, a nano-wire's elongated shape (high aspect ratio) allows for a conductive film to be achieved at a far lower particle density, resulting in fewer inter-particle junctions.<sup>23</sup>

This work describes the fabrication of transparent, conductive, and flexible alternatives to ITO and FTO glass substrates for optoelectronic applications such as PV. A composite comprising of BC and binding agents (PVA or PEO) formed the transparent and flexible

substrate. An optimized AgNW coating provided a conductive network to the flexible film that was able to preserve the transparency of the cellulose-based film.

## 2 | RESULTS AND DISCUSSION

### 2.1 | Biosynthesis of BC and BC microfibers

BC producing bacteria was cultivated from commercially available Kombucha tea. Kombucha tea is an age-old, slightly acidic health beverage, globally consumed for its richness in probiotics and nutrients.<sup>24</sup> When supplemented with black or green tea and sufficient amounts of sugar, the Kombucha tea transforms into a medium that feeds and produces a symbiotic culture of bacteria and yeast (SCOBY).<sup>25</sup> The bacteria and fungus in the Kombucha present a powerful symbiosis that can inhibit the growth of potentially contaminating bacteria.<sup>26</sup> In this study, the SCOBY was responsible for BC growth (Figure 1).

Once the SCOBY developed (at least 1 cm thick), it was introduced into a modified Hestrin and Schramm (HS) medium that contained macro and micronutrients that assist in the growth of the microorganisms. A static growth approach was adopted to cultivate the BC. After 3 days, a thin, clear, gelatinous layer (i.e., the cellulose) was observed at the surface of the HS medium, sprouting from the SCOBY. The biosynthesis of BC is a multistep process that relies on several key enzymes that control cellulose synthesis.<sup>27</sup> During the biosynthesis, cellulose building blocks are secreted through the pores in the bacteria's cell wall and aggregate into pure, organized, 3D

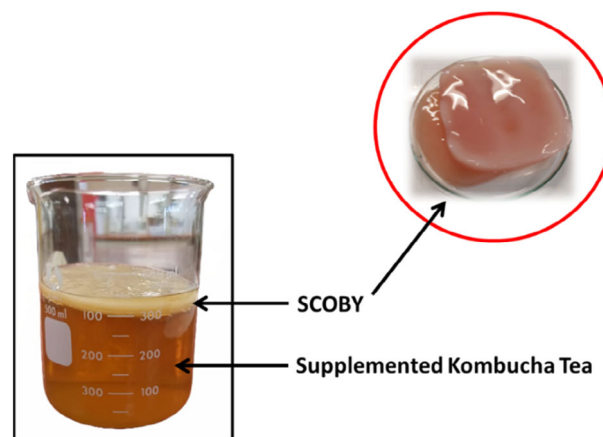


**FIGURE 1** Supplemented Kombucha tea with grown symbiotic culture of bacteria and yeast (SCOBY); (inset) SCOBY used in the biological growth of bacterial cellulose (BC). [Color figure can be viewed at [wileyonlinelibrary.com](http://wileyonlinelibrary.com)]

cellulose fibers that are stabilized by inter- and intramolecular hydrogen bonds.<sup>27–29</sup>

The BC growth was monitored daily and grew into a pellicle that conformed to the container's shape. After a 2–3 week growth period, the BC pellicle appeared as a thicker, translucent, cream-yellow colored gelatinous substance (Figure 2). The yellow color of the BC pellicle is due to surface impurities and bacterial cellular residues and was removed using alkaline treatment with NaOH.<sup>30</sup> Bleaching with NaClO was done after alkaline treatment to remove chromophores and phenolic compounds. The bleaching processes improved the appearance and transparency of the resultant films.<sup>31</sup>

Figure 3a shows the scanning electron microscopy (SEM) micrograph of the BC. The BC accumulated as a

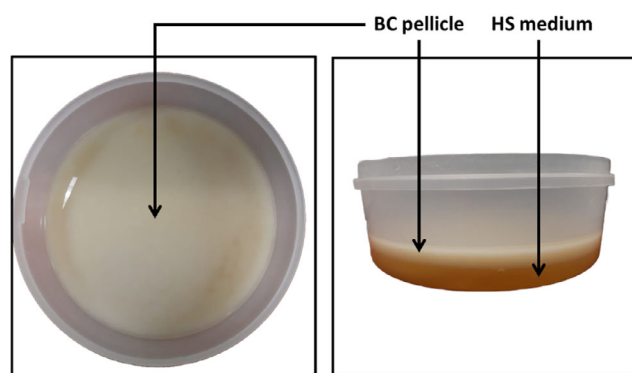


FIGURE 2 Bacterial cellulose (BC) biosynthesized from the symbiotic culture of bacteria and yeast (SCOBY) in the Hestrin and Schramm (HS) medium. [Color figure can be viewed at [wileyonlinelibrary.com](http://wileyonlinelibrary.com)]

gelatinous membrane at the interface between the culture medium and air. The micrograph shows that the surface of the BC film appears as a randomly assembled 3D network of entangled fibers. The individual cellulose fibrils were visible and had an average diameter of  $61.73 \text{ nm} \pm 10.39 \text{ nm}$  (Figure 3b).

The BC pellicle was liquidized into a pulp, which was subjected to acid hydrolysis to obtain micro-sized BC fibers (BMF). Acid hydrolysis typically leads to the diffusion of hydronium ions ( $\text{H}_3\text{O}^+$ ) into cellulose fibrils (Figure S1), causing the hydrolytic cleaving of glycosidic linkages within cellulose molecular chains. This hydrolysis breaks down the hierarchical structure of the cellulose into microfibrils and induces repulsive electrostatic forces between negatively charged microfibrils allowing for colloidal stability and dispersion in water.<sup>32,33</sup> Transmission electron microscope (TEM) micrographs and size distribution curves of the BMF confirmed that the long BC fibers were indeed hydrolyzed to a measurable micrometer scale, with an average length of  $1.35 \mu\text{m} \pm 0.2 \mu\text{m}$  (Figure S2). The average width of the BMF was  $60.37 \text{ nm} \pm 11.24 \text{ nm}$ . In comparison to the BC, the differences in the measured widths are negligible and indicate that the hydrolysis only reduced the length of the fibers and not the width.

## 2.2 | BMF-polymer film fabrication

Two outcomes were identified when processing films consisting of 100% BMF, (i) at low BMF concentrations, the BMF films were unable to retain their shape and

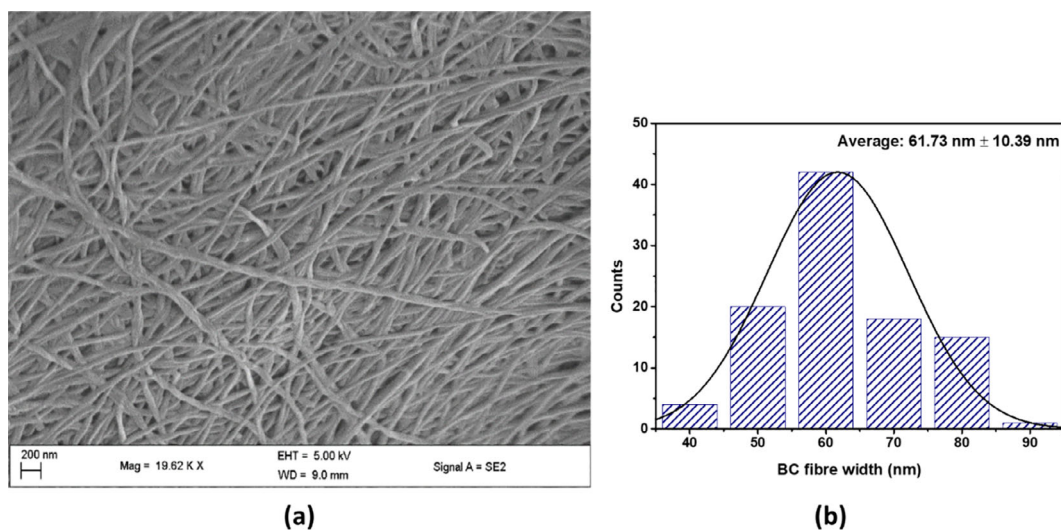


FIGURE 3 (a) Scanning electron microscope (SEM) micrograph of bacterial cellulose (BC) film and (b) size distribution curve of the bacterial cellulose (BC) fiber diameters. [Color figure can be viewed at [wileyonlinelibrary.com](http://wileyonlinelibrary.com)]

readily disintegrated, and (ii) at high BMF concentrations, the films formed were brittle and unsuitable for the applications mentioned above. Therefore, PVA and PEO were selected as reinforcing and binding agents to improve the mechanical properties and processing capacity of BMF films.

In addition, the PVA and PEO polymers assist in maintaining the original character of cellulose films concerning transparency, biodegradability, and economic feasibility. As an additive to BMF, the amount of PVA and PEO used to fabricate the films did not exceed that of BMF. Ultrasonication was used to physically crosslink the BMF to the respective polymer to form the composite film. The crosslinking takes place via intermolecular interactions between the hydroxyl groups on the cellulose and the hydroxyl groups on PVA or the ether groups on PEO.<sup>34,35</sup>

The composite nature of the BMF-polymer films was characterized by X-ray diffraction (XRD) analysis as shown in Figure 4. Three broad peaks were identified at  $2\theta = 14.4^\circ$ ,  $16.8^\circ$ , and  $22.9^\circ$  for BMF, and were assigned to the (1 0 1), (1  $\bar{0}$  1) and (0 0 2) planes. Like cellulose,

PVA is semi-crystalline and shows a single broad peak at  $2\theta = 19.48^\circ$  and a shoulder at  $2\theta = 20.84^\circ$ . The intense peak at  $19.48^\circ$  was assigned to a mixture of 10 $\bar{1}$  and 101 reflections,<sup>36–38</sup> and the shoulder at  $20.84^\circ$  was assigned to the (2 0 0) plane from a monoclinic unit cell.<sup>39</sup>

According to the  $2\theta$  values (Table S1), films A–E exhibit similar diffraction peaks corresponding to the (2 0 0) plane of cellulose and the (10 $\bar{1}$ ) and (101) planes for PVA. These PVA peaks become prominent with increasing PVA ratios. The appearance of peaks characteristic to BMF and PVA in the diffractograms for films A–E confirm their presence in the composite. Furthermore, subtle shifts in  $2\theta$  values in the XRD spectra can be tentatively assigned to a possible interaction between the BMF and PVA.

The diffractogram for the pure PEO film (Figure 4b) demonstrates two crystalline peaks at  $2\theta = 19.35^\circ$  and  $23.59^\circ$  (Table S2), which are attributed to the (1 2 0) and (1 1 1) planes of a PEO monoclinic crystal structure.<sup>40,41</sup> These diffraction peaks were generated by combining the polyether side chains and intermolecular interactions between PEO chains via H-bonding.<sup>42–44</sup> The sharpness

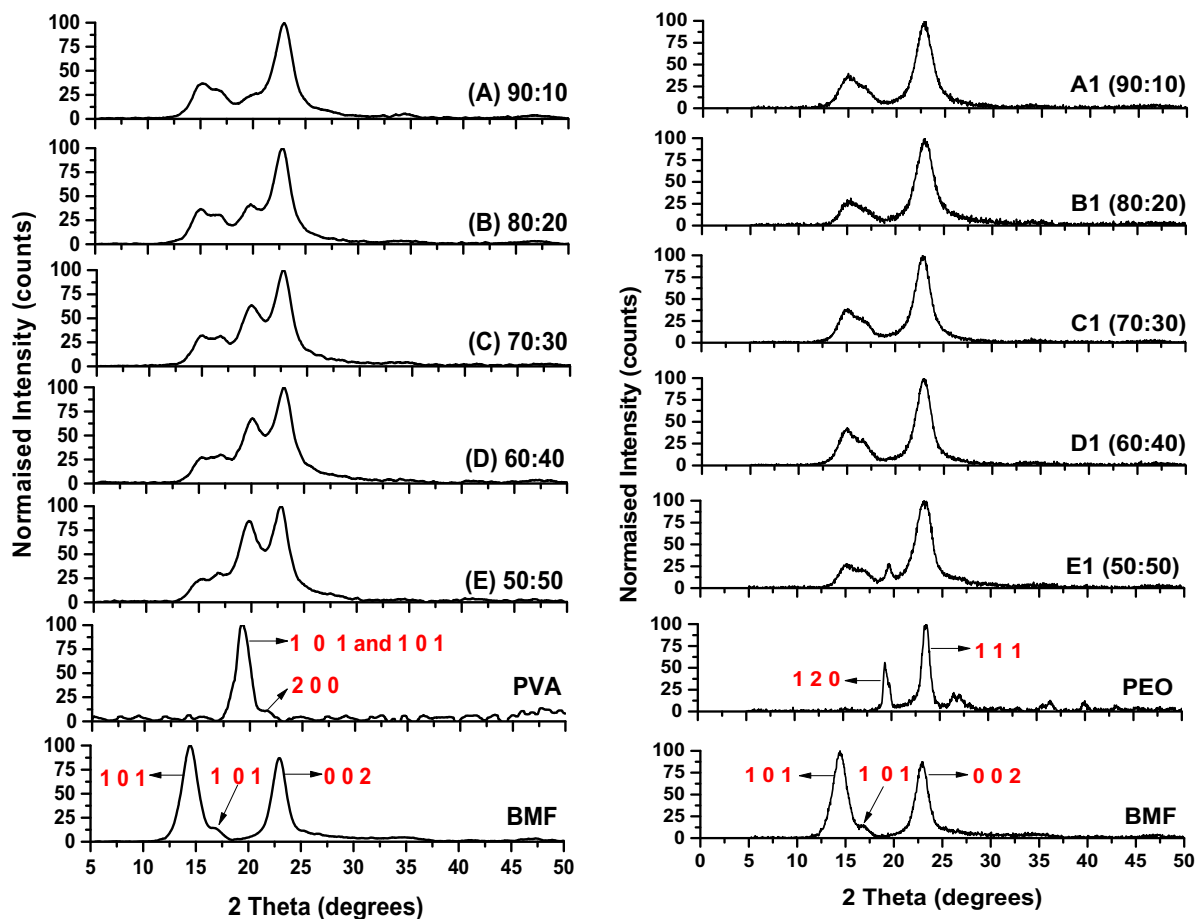


FIGURE 4 X-ray diffraction (XRD) analysis diffractograms of (a) pure bacterial cellulose (BC) film, pure PVA film and composite films A–E and (b) pure BC film, pure PEO film and composite films A1–E1. [Color figure can be viewed at [wileyonlinelibrary.com](http://wileyonlinelibrary.com)]

of these peaks signifies the relatively high degree of crystallinity of the PEO, but the simultaneous presence of a halo region between  $15^\circ$  and  $30^\circ$  indicates a semi-crystalline nature of PEO.<sup>45,46</sup> The PEO diffractogram also shows less intense peaks at  $2\theta = 36.24^\circ$  and  $39.93^\circ$  that have been reported in other studies.<sup>47</sup> Peaks associated with the (1 0 1) and (1  $\bar{0}$  1) planes of BMF can be seen in films A1–E1, but have experienced reduced intensities and shifting to higher  $2\theta$  values. Due to the (2 0 0) plane associated with BMF at  $2\theta = 22.94^\circ$  and the (1 1 1) plane associated with PEO at  $2\theta = 23.59^\circ$ , the A1–E1 films have an ambiguous peak ranging between  $22.8^\circ$  and  $23.2^\circ$  that cannot be precisely distinguished to BMF or PEO, even if deconvoluted. Film A5, containing the highest amount of PEO, did produce a diffraction peak at  $2\theta = 19.66^\circ$ , which can be associated with the (1 2 0) plane of PEO. The shift in  $2\theta$  values, change in peak intensity, and shape confirm the composite nature of the films and possible interactions between BMF and PEO.

### 2.2.1 | Mechanical properties

Dynamic mechanical analysis (DMA) studies were carried out to evaluate mechanical properties of the films. As separate entities, BC is characterized by high tensile strength and has reported Young's Modulus ( $E$ ) ranging from 1 MPa to over 100 GPa while PVA and PEO have elastic properties which are expected to improve the elasticity and flexibility of the composite films.<sup>48</sup> Considering the purpose and function of the composite films,  $E$  was deduced from stress–strain curves to evaluate the elastic effect imparted by PVA and PEO toward the BMF-based films (Figures S3–S7).

A high  $E$  value represents a stiff material, while a comparatively lower  $E$  value represents a more elastic material. The  $E$  values (Table S4) were extracted from the linear region ( $R^2$  values of  $\geq 0.998$ ) of the respective stress–strain curves. The BMF film produced the highest  $E$  value of 74.13 MPa, while PVA and PEO films produced the lowest  $E$  values of 2.155 MPa and 4.303 MPa respectively, as expected. The BMF and film A generated stress–strain curves with a shape that describes brittle materials, while the PVA and the B–E films generated stress–strain curves that identify with ductile materials. The increasing amounts of PVA in films A to E gradually lowered  $E$  and appeared to have improved the elasticity and, by extension, the flexibility of the films. This is a direct result of the crosslinking between the BMF and PVA, without PVA being the major contributing material.

Although all the BMF-PEO based films (A1–E1) displayed brittle behavior when assessing the shape of the

stress–strain curves, it is noticed that increasing amounts of PEO reduces  $E$  in the films. This confirms interactions between BMF and PEO, where PEO imparts elastic behavior to the films.

To compare, the BMF-PEO films at any given ratio yielded slightly higher  $E$  values than their BMF-PVA counterparts, suggesting that although PEO plays a role in providing flexibility to the films, it does not contribute as much as PVA. This is reaffirmed by the higher  $E$  value obtained by pure PEO than pure PVA. The molecular weights of the respective polymers may have influenced the flexibility of the BMF-polymer composite films. The molecular weight of the PEO used was greater than that of the PVA, therefore, may not have contributed to the flexibility of the films to the same extent as the lower molecular weight PVA polymer. The percentage change (%) in  $E$  between the pure BMF film and the A–E and A1–E1 films is shown in Figure 5.

The graph established that the change observed in the A–E films is much greater than the change recorded for the A1–E1 films. Also noticeable is a sharp increase ( $\geq 21\%$ ) in the % change from 80:20 to 70:30, followed by relatively smaller % changes between 70:30, 60:40 and 50:50 for both sets of films. Considering mechanical properties only, Figure 5 indicates that the optimum ratio for fabricating the composites is a mixture comprising 70% BMF and 30% polymer.

A closely related term to  $E$  is “yield strength” ( $\sigma_Y$ ). Yield strength is the point on the curve at which the applied stress induces plastic deformation in the films. A standard practice referred to as the “0.2% method” was implemented to quantify the stress needed to cause

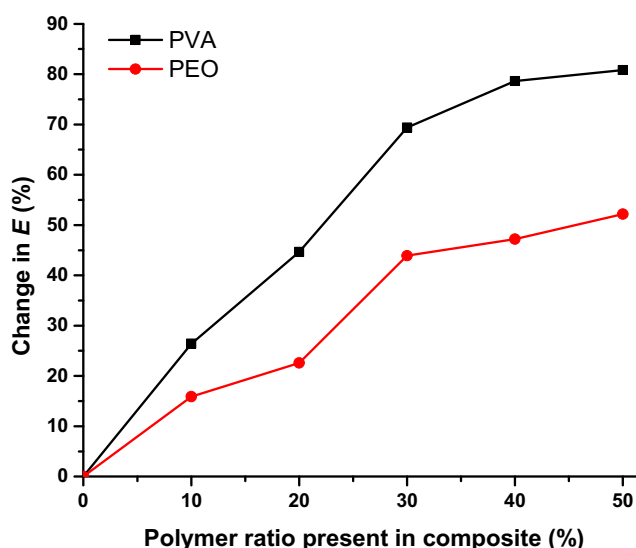


FIGURE 5 Percentage change in Young's Modulus ( $E$ ) at different polymer ratios present in A–E and A1–E1 composite films. [Color figure can be viewed at [wileyonlinelibrary.com](https://onlinelibrary.wiley.com/doi/10.1002/app.54090)]

permanent strain. As seen in all the stress–strain curves (Figures S3–S7), a brown dashed line was constructed perpendicular to the linear region and the point of interception at the original curve is called the “0.2% offset yield strength.” It is estimated that before the  $\sigma_Y$ , the linear behavior of the films is quite predictable, but after the  $\sigma_Y$ , the films start to deviate from linearity and their behavior becomes variable. Further evaluation of the stress–strain curves indicates that as the amount of PVA increases in the films, the lower the  $\sigma_Y$  value. This indicates that as a consequence of improving the flexibility of the film, the presence of PVA and PEO also lowers the amount the stress needed to cause permanent strain deformation and is an important consideration when determining the optimum ratio for the composite film. Additionally, soda-lime glass is used to manufacture commercially available ITO and FTO glass substrates. Soda-lime glass has an  $E$  ranging between 68 and 72 GPa and  $\sigma_Y$  of ranging between 35 and 60 MPa.<sup>49</sup> One of the key features required from alternative TCs is flexibility. When compared to soda-lime glass, the A–E and A1–E1 composite films show superior flexibility and can maintain similar  $\sigma_Y$  values at appropriate composition ratios.

### 2.2.2 | Thermal properties

Thermogravimetric analysis (TGA) was used to investigate the thermal performance of pure BMF, PVA, PEO and the physically crosslinked composite films A–E and A1–E1. The thermograms (Figures S8 and S9) for the A–E and A1–E1 films reveal three main weight-loss regions. An overview of the thermograms show that the thermal stability of the composites films is a product of the individual components in the respective films, that is, BMF, PVA, or PEO. This suggests that the BMF and the polymers were blended homogeneously, thus both contributing to the overall thermal stability of the films. When comparing blends, the thermograms indicates that the A1–E1 films have better thermal stability throughout the first and second weight-loss regions and display higher decomposition temperatures (Table S5). A possible explanation for this is that PEO improves thermal properties between 30 and 230°C, whereas PVA improves thermal properties in the third region at higher temperatures.

Despite both sets of composite films displaying good thermal stability between the 0 and 180°C region, the thermograms indicate that the composite films are unsuitable for applications or processing techniques requiring temperatures exceeding  $\sim 180^\circ\text{C}$ . The films experienced major decomposition between 187 and 216°C (Table S5). This drawback limits the use of the films in heat-intensive applications (e.g., lasers), processing at high

annealing temperatures, and using heat-intensive coating methods such as sputtering and thermal evaporation. The glass counterparts, however, are advantageous in this regard as they can withstand comparatively higher temperatures.

### 2.2.3 | Optical properties and film optimization parameters

Glass is the traditional substrate used for ITO and FTO deposition, and the most inherent property of glass is transparency. The transparency of a material indicates the amount of electromagnetic radiation that can transmit through the material and is an important property to be considered when fabricating materials for optoelectronic devices. The fabricated composite films, A–E and A1–E1, are visually transparent and smooth, Figure S10. The optical transmittance spectra obtained from UV–vis spectroscopy for the pure BMF, PVA, and PEO films and respective composite films are shown in Figure S11. The transmission spectroscopy measurements were performed between 300 and 800 nm to capture light transmission largely within the visible spectrum and a portion of the UV spectrum.

Pristine BMF films displayed excellent transmittance by maintaining  $\sim 99\%$  transmission of light between 800 and 560 nm, thereafter, it plateaus at 92% between 400 and 300 nm. These transmission results are better than commercial soda-lime glass which has been reported between 70% and 85% within the visible region.<sup>50–52</sup> In comparison to the pure BMF film, pure PVA and PEO films showed noticeably lower transmissions. All the composite films (A–E and A1–E1) showed decreasing light transmissions as the amount of polymer in the films increased. For example, film A has a composition of 90% BMF and 10% PVA and maintained  $\sim 95\%$  of transmission between 800 and 500 nm. In contrast, film D has a composition of 60% BMF and 40% PVA and showed reduced transmission, maintaining  $\sim 89\%$  transmission in the same region. Therefore, the greater the amount of polymer present in the composite, the lower the transmission of light by the film. This further validates the interaction between the BMF and the polymers in the composite films.

A balance between durability (physical and thermal) and transparency needs to be considered to determine the films' optimum composition for the respective optoelectronic-based applications. The ratio of BMF to polymer strongly influences both properties. Increasing the amount of polymer improves flexibility and reduces film deformation but it also lowers light transmission. The optimum ratio of BMF to polymer with regards to

$E$  is 70:30 (Figure 5). At this ratio, films C and C1 show transparency in the 800–400 nm region at  $\sim 91\%$ – $90\%$  and  $\sim 87\%$ – $81\%$ . These are favorable transmission ranges in comparison to pure BMF and commercial glass.

Despite showing the same decreasing light transmission trends, the A–E films proved to be better at transmitting light at varying ratios than the A1–E1 films. The composites exhibit their suitability as materials capable of replacing common, transparent, and brittle materials such as glass.

### 2.3 | Synthesis of AgNWs

A polyol reduction was used to synthesize the conductive AgNWs. During this process, the  $\text{Ag}^+$  precursor was reduced by a polyol at elevated temperatures. A capping agent was also used to control the shape and stability of the final nanowire product.<sup>53</sup> The polyol reduction was supplemented with self-seeding additives to promote the selective formation of AgNWs during the nucleation process.

The surface morphology of the AgNWs was studied using SEM which confirmed the nanowire morphology of the AgNWs. The images showed uniform wire-like structures with high aspect ratios (Figure 6a,b). From TEM images (Figure S12), it is noticed that the nucleation growth process formed other morphologies as well. Although several washing and centrifugation steps were undertaken, there remained a relatively low percentage of other nanoparticles. Dimension distribution curves reflect the high aspect ratio of the nanowires, as the average width and length of the nanowires were calculated to be  $64.17 \pm 10.63$  nm and  $2.09 \pm 0.97$   $\mu\text{m}$ .

To characterize and compare the conductive properties of AgNWs to ITO and FTO, the energy bandgap ( $E_g$ ) of the AgNWs was calculated directly from the UV–vis spectra using Tauc's equation.<sup>54,55</sup> Using  $n = 2$ , the  $E_g$  of the AgNWs was observed at 2.01 eV. Electrical conduction in any material relies on the electron population and movement between the valence and conduction bands. Therefore, the size of the  $E_g$  is an important parameter when characterizing the conductive properties of a material. In comparison to the  $E_g$  of ITO (i.e., 3.50–4.35 eV)<sup>56–58</sup> and FTO (i.e., 3.14–4.25 eV),<sup>59–61</sup> the synthesized AgNWs are better conducting materials as the energy required to excite an electron from the valence band to the conduction band and create charge carriers for current generation is lower than required for ITO and FTO.

### 2.4 | BMF-polymer-AgNW film fabrication

To preserve film transparency while achieving competitive electrical resistance to commercial TCs, it was necessary to optimize the AgNW coating. The coating was performed using a two-step transfer method as described in Figure 7.

The first transfer of the AgNW coating occurred between the mixed cellulose ester (MCE) membrane and printed circuit board (PCB) heat transfer paper (Figure S13). The second transfer occurred between the PCB heat transfer paper (Figure S14) and the BMF-polymer films (Figure S15). The AgNW mass range (0.10–0.50 mg) was selected by performing preliminary

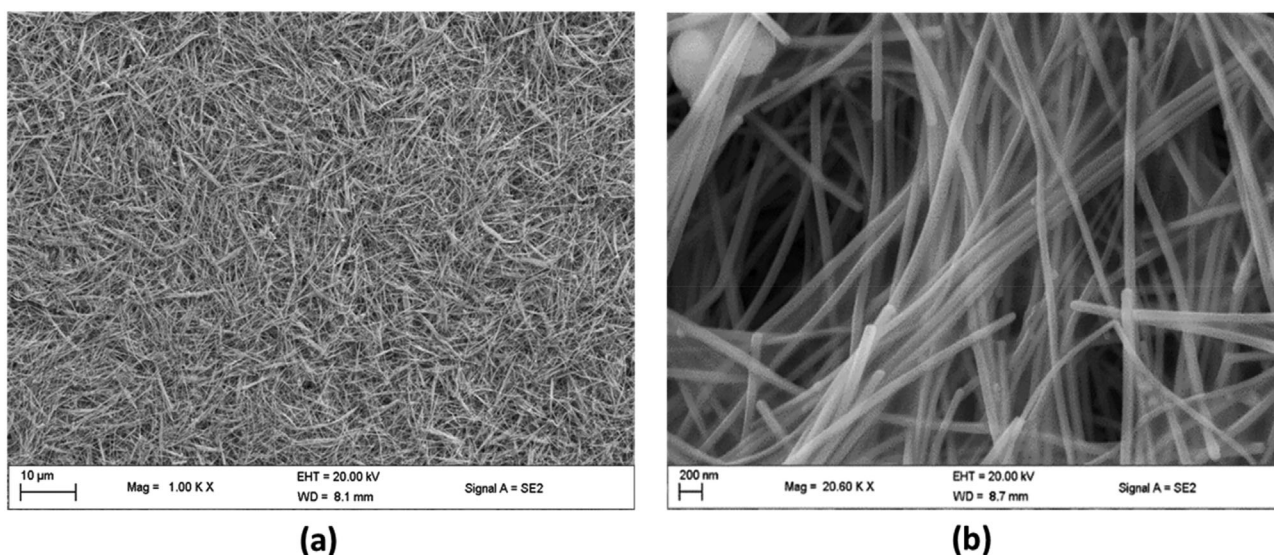


FIGURE 6 Scanning electron microscope (SEM) micrographs of AgNWs at a magnification of (a) 1.00 K X and (b) 20.00 K X.

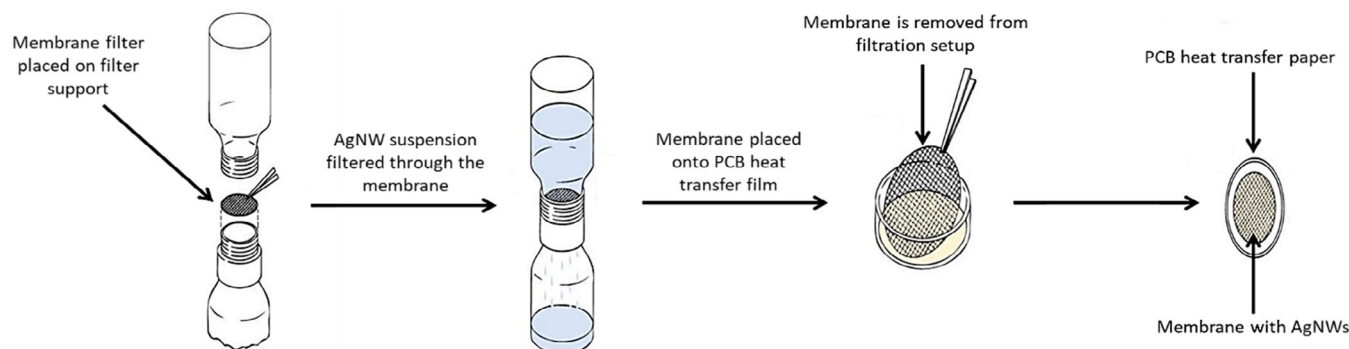


FIGURE 7 Transfer method used to coat the bacterial cellulose microfiber-PVA (BMF-PVA) and BMF-PEO films with AgNWs. [Color figure can be viewed at [wileyonlinelibrary.com](https://onlinelibrary.wiley.com/doi/10.1002/app.54090)]

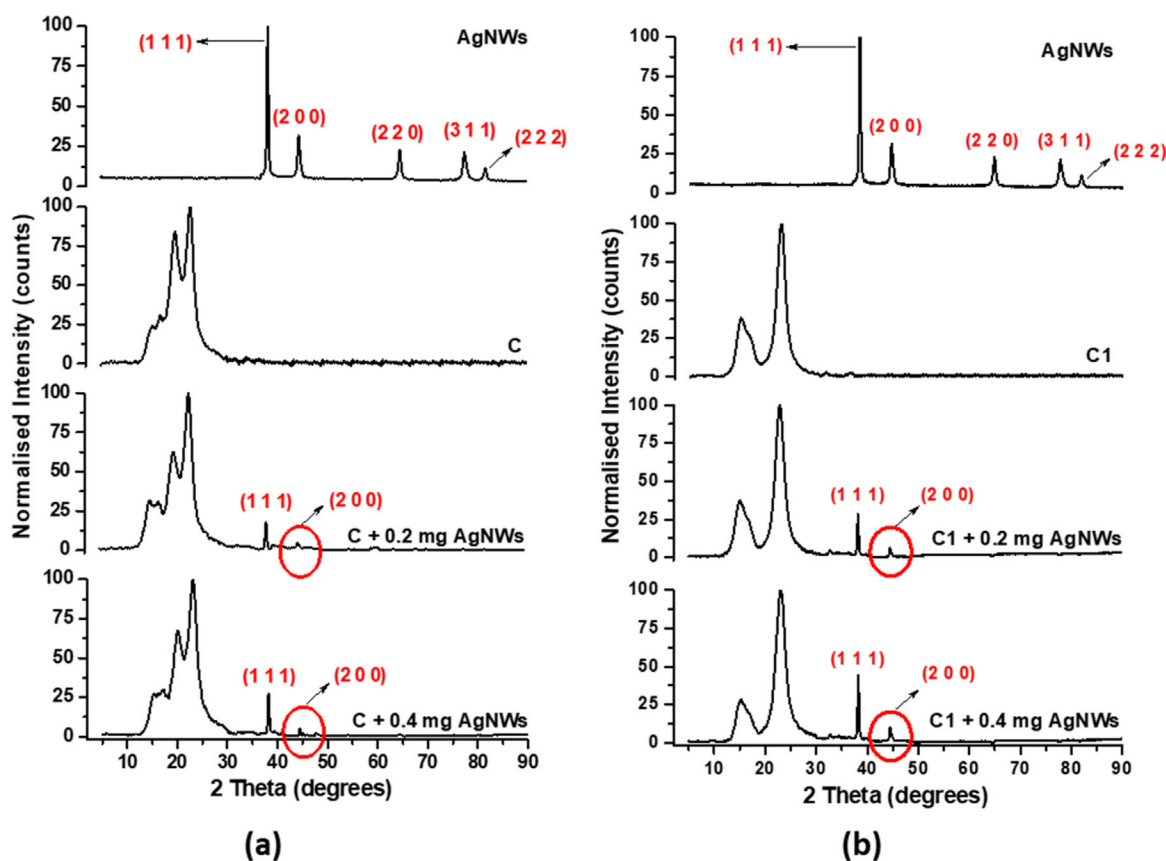


FIGURE 8 X-ray diffraction (XRD) analysis diffractograms of AgNWs, bacterial cellulose microfiber (BMF)-polymer films (C and C1) and, BMF-polymer-AgNWs films (C + 0.20 AgNWs, C + 0.40 AgNWs, C1 + 0.20 AgNWs and C1 + 0.40 AgNWs). [Color figure can be viewed at [wileyonlinelibrary.com](https://onlinelibrary.wiley.com/doi/10.1002/app.54090)]

resistance measurements with a standard multi-meter, directly on AgNW coated MCE membrane filters.

XRD was used to confirm the transfer of the AgNWs onto the BMF-polymer films (Figure 8). The diffractogram of AgNWs showed five diffraction peaks at  $2\theta = 38.29^\circ$ ,  $44.50^\circ$ ,  $64.60^\circ$ ,  $77.56^\circ$ , and  $81.65^\circ$  which were indexed to the (1 1 1), (2 0 0), (2 2 0), (3 1 1), and

(2 2 2) reflections of face-centered cubic structure of silver.<sup>62</sup> For comparative purposes, C and C1 films with low (0.20 mg) and high (0.40 mg) AgNW loading were characterized. The AgNW-coated C and C1 films displayed peaks characteristic of their original BMF-polymer compositions and new peaks associated with AgNWs. The AgNW-coated C and C1 films showed



peaks associated with the (1 1 1) and (2 0 0) Ag planes at the low and high AgNW loadings establishing the BMF-polymer-AgNW composition of the films. There are minor  $2\theta$  shifts between the original C and C1 films, and the AgNW-coated films, typically observed for composite materials (Table S6).

The SEM micrographs of the BMF-PVA-AgNWs and BMF-PEO-AgNWs are displayed in Figure 9a–d. The C and C1 films with a low (0.20 mg) and high (0.40 mg) Ag loading were imaged. The micrographs confirm the transfer of the AgNW network onto the surface of C and C1 films. The AgNWs maintained their nanowire morphology upon transfer; however, the micrographs revealed some areas of uneven AgNW distribution across the surface of the film (Figure 9b,d). From SEM micrographs, areas of poor AgNW distribution is observed, which directly impact resistivity measurements (Section 2.4.1).

#### 2.4.1 | Electrical resistivity properties

The electrical resistivities of the respective AgNW-coated films were recorded using an in-house constructed apparatus (Figure S16) over a surface area of  $1\text{ cm}^2$ .<sup>63</sup> The resistivities of ITO and FTO measured with the self-designed apparatus compare well to their reported values of  $\sim 15\ \Omega/\text{sq}$  and  $\sim 7\ \Omega/\text{sq}$ , as specified in Section 5.1 and those reported in literature.<sup>56,64,65</sup>

This indicates the measurement protocol gives reliable data to compare with the AgNW-coated films. As shown in Table 1, the resistivities measured for the BMF-PVA-AgNW and BMF-PEO-AgNW films increase as the Ag loading decreases. This was expected, as lower Ag loadings hinder current flow due to decreased physical contact of the AgNWs that are dispersed across the surface of the films.

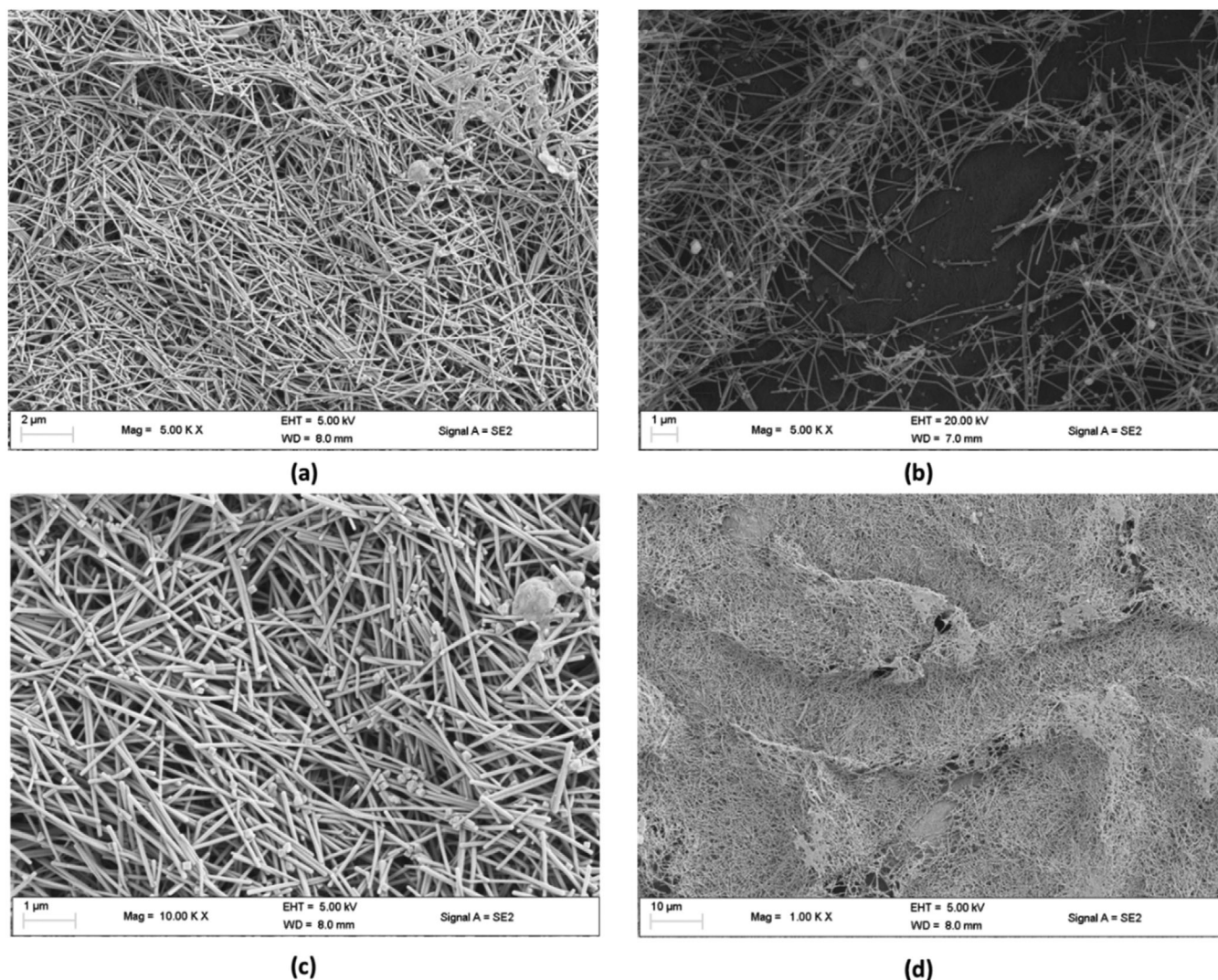


FIGURE 9 Scanning electron microscope (SEM) micrographs of (a) bacterial cellulose microfiber (BMF)-PVA-AgNW (0.40 mg AgNWs) at 5.00 K X, (b) BMF-PVA-AgNW (0.20 mg AgNW) at 5.00 K X, and BMF-PEO-AgNW (0.40 mg AgNW) at (c) 10.00 K X and (d) 1.00 K X.

TABLE 1 Electrical resistivity and non-uniformity factor (NUF) values for BMF-PVA-AgNW and BMF-PEO-AgNW films.

AgNW (mg)	Resistivity ( $\Omega/\text{sq}$ )		NUF	
	BMF-PVA-AgNW	BMF-PEO-AgNW	BMF-PVA-AgNW	BMF-PEO-AgNW
0.10	40.69 $\pm$ 2.48	41.55 $\pm$ 3.32	0.2146 $\pm$ 0.00605	0.1879 $\pm$ 0.0299
0.15	21.07 $\pm$ 1.35	22.44 $\pm$ 3.03	0.1899 $\pm$ 0.0160	0.1569 $\pm$ 0.0244
0.20	9.462 $\pm$ 0.588	9.388 $\pm$ 1.37	0.1844 $\pm$ 0.0133	0.1218 $\pm$ 0.0166
0.30	8.955 $\pm$ 0.878	8.848 $\pm$ 0.976	0.1779 $\pm$ 0.0142	0.1174 $\pm$ 0.0127
0.40	3.248 $\pm$ 0.451	3.588 $\pm$ 0.571	0.1586 $\pm$ 0.0121	0.1116 $\pm$ 0.0103
0.50	2.633 $\pm$ 0.270	2.848 $\pm$ 0.468	0.1101 $\pm$ 0.0148	0.1102 $\pm$ 0.0115
ITO	11.14 $\pm$ 0.775		0.06598 $\pm$ 0.0112	
FTO	8.037 $\pm$ 0.467		0.05395 $\pm$ 0.0118	

Abbreviations: BMF, bacterial cellulose microfiber; FTO, fluorine-doped tin oxide; ITO, indium-tin oxide.

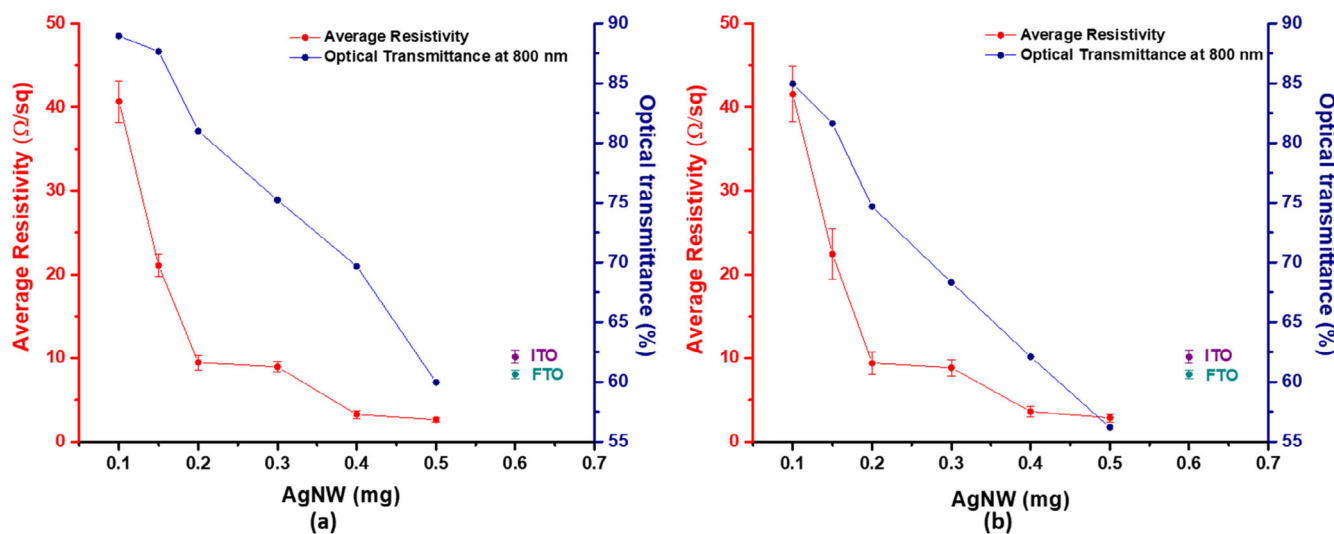


FIGURE 10 Average resistivity versus optical transmittance at 800 nm at different AgNW loadings for (a) bacterial cellulose microfiber (BMF)-PVA-AgNW and (b) BMF-PEO-AgNW films. [Color figure can be viewed at [wileyonlinelibrary.com](https://onlinelibrary.wiley.com/doi/10.1002/app.54090)]

In comparison, the BMF-PVA-AgNW and BMF-PEO-AgNW films produced similar resistivity values at the varying AgNW loadings. Films coated with higher amounts of Ag (0.50 and 0.40 mg), produced low resistivities between 2.633 and 3.588  $\Omega/\text{sq}$  while films coated with lower amounts of Ag (0.15 and 0.10 mg), produced significantly higher resistivities between 21.07 and 41.55  $\Omega/\text{sq}$ , respectively.

Figure 10 is a graphical comparison between the average resistivity of the AgNW-coated films to the optical transmission at 800 nm at varying AgNW loadings. Between the BMF-PVA-AgNW and BMF-PEO-AgNW films, it was expected that the latter set of films would show slightly lower percentages of light transmission as initial transmission investigations (See Section 2.2.3) indicated that the BMF-PVA films display better light-transmitting properties.

Both graphs highlight the compromise between the transparency and conductivity of the films. Although the AgNWs are responsible for the film's conductive properties, higher Ag loadings on the films result in decreased transparency.

The BMF-PVA-AgNW and BMF-PEO-AgNW films coated with 0.50, 0.40, 0.30, and 0.20 mg of Ag can compete with the resistivities of commercial ITO and FTO substrates, which measured 10.14  $\pm$  0.7751  $\Omega/\text{sq}$  and 8.037  $\pm$  0.4667  $\Omega/\text{sq}$ , respectively. The 0.15 and 0.10 mg AgNW coated films display resistivities that are  $\sim$ 4 times and  $\sim$ 5 times greater than ITO and FTO resistivities.

When considering the optical transmittance of the BMF-PVA-AgNW and BMF-PEO-AgNW films, films loaded with 0.20 and 0.30 mg of Ag can compete with the optical transmittance displayed by ITO and FTO. The optical transmittance data combined with the resistivity

data indicate that the optimum Ag loading for BMF-PVA-AgNW and BMF-PEO-AgNW films is 0.20 mg. The BMF-PVA-AgNW films loaded with 0.20 mg of Ag show optical transmittance ranging from 81% to 71% between the 800 and 350 nm region while maintaining an average resistivity of  $9.462 \pm 0.588 \Omega/\text{sq}$ . The BMF-PEO-AgNW films loaded with 0.20 mg of Ag show optical transmittance ranging from 73% to 65% between the 800 and 350 nm region and recorded average resistivity values of  $9.388 \pm 1.375 \Omega/\text{sq}$ .

Under ambient coating conditions, the deposition of nanoparticles onto a substrate is influenced by mass transport under a concentration gradient commonly referred to as the “coffee ring effect.”<sup>66,67</sup> The nanoparticles tend to aggregate at the peripheral area of the substrate, where the colloidal nanoparticle solution evaporates faster due to temperature variations.<sup>68–70</sup> The varying evaporation rates cause an inhomogeneous coating on the surface of the substrate. The deposition method described in this work may have been subjected to the coffee ring effect during the filtration of the AgNWs onto the membrane filters. Although steps were taken to prevent inhomogeneous coatings, the sensitive nature of the membrane filter allowed only for natural drying after filtration. This may have introduced inhomogeneous or uneven AgNW coatings transferred to the BMF-polymer films during the transfer method.

Ideally, the Ag coating onto the BMF-polymer films is expected to be random and even, with a narrow size distribution (SD) for optimum uniformity. Jia and co-workers derived a non-uniformity factor (NUF) to evaluate the SD of the sheet resistance of the films in cases such as this, rather than using typical SD statistics. The NUF equation is seen in Equation (1)<sup>66</sup>:

$$\text{NUF} = \sqrt{\frac{1}{n} \frac{\sum_{i=1}^n (R_i - \bar{R})^2}{\bar{R}^2}} \quad (1)$$

where  $n$  is the number of measurements obtained from the film at different sites,  $R_i$  is the measurement resistance and  $\bar{R}$  is the average resistance of all the measurements. The smaller the calculated NUF, the more uniform the film is. The NUF values were calculated (Table 1) and are graphically represented in Figure 11.

The NUF values for the BMF-PVA-AgNW and BMF-PEO-AgNW films are  $<0.22$  with negligible deviation ( $<0.03$ ). This indicates that the described transfer method produces reproducible and uniform AgNW coatings on BMF-PVA and BMF-PEO films. It is noticeable that like the resistivity measurements, the NUF values increase as the amount of Ag decreases, indicating that the films become relatively less uniform with reduced amounts of Ag. When the distribution uniformity decreases, it is difficult for the AgNWs to form continuous and effective conductive pathways across the surface of the BMF-polymer substrates. The NUF values in Table 1 are comparable to the NUF values of ITO ( $0.06598 \pm 0.02287$ ) and FTO ( $0.05395 \pm 0.01278$ ) substrates measured in this work.

### 3 | COMPARATIVE OVERVIEW BETWEEN BMF-PVA-AgNW AND BMF-PEO-AgNWs FILMS

The primary use of PVA and PEO additives was to bind the BMF and provide structural support via crosslinking to the resultant films without being the major contributor

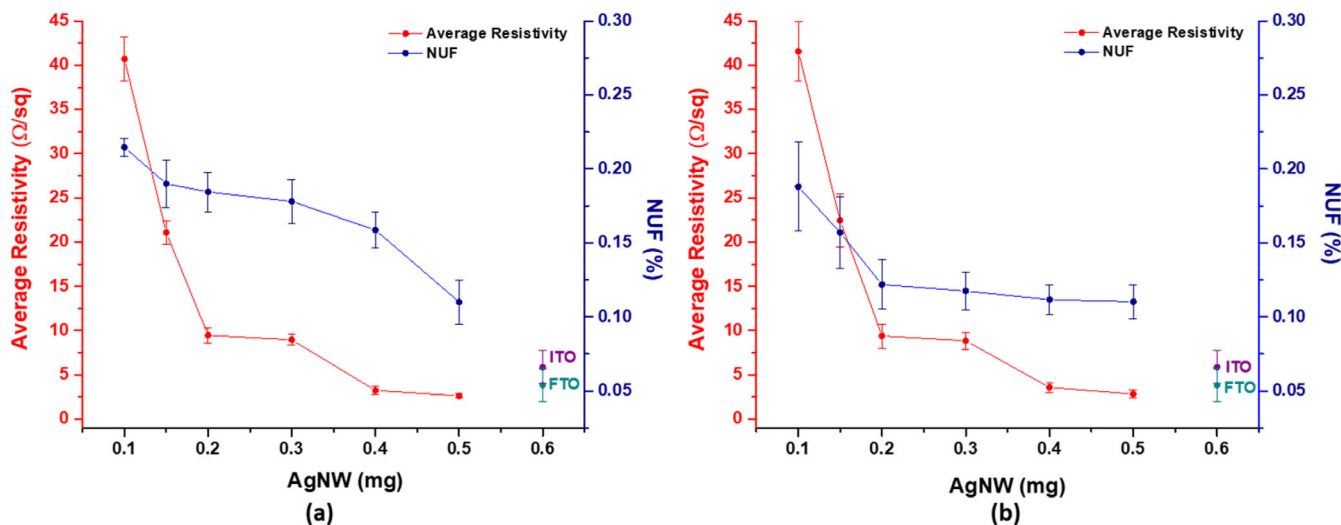


FIGURE 11 Average resistivity versus non-uniformity factor (NUF) of the (a) bacterial cellulose microfiber (BMF)-PVA-AgNW and (b) BMF-PEO-AgNW films at different Ag loadings. [Color figure can be viewed at [wileyonlinelibrary.com](http://wileyonlinelibrary.com)]

to the films. The BMF-PVA and BMF-PEO films interacted well, forming smooth, visually transparent, and flexible self-assembled films. According to measured  $E$  values, the addition of PEO to the BMF created films that displayed flexibility but appeared more ductile than BMF-PVA films. Regarding optical transmittance, the BMF-PVA films displayed better optical transmittance than the BMF-PEO films within the 800–350 nm region. The final films, BMF-PVA-AgNW and BMF-PEO-AgNW showed marginal differences in the measured resistivities and AgNW loading uniformity. The differences observed between the films are based on structural and optical properties and can be applied to applications accordingly for their strengths. The fabrication of the BMF-PVA-AgNW and BMF-PEO-AgNW films is reproducible and can be considered useful polymer-based TCs prototypes for optoelectronic applications.

## 4 | CONCLUSION

This study reports on the fabrication of conductive, transparent, and flexible films as a composite of BMF, a polymer (PVA or PEO) as a binding and reinforcing agent, and AgNWs as the conductive material. The PVA and PEO polymers contribute toward improved flexibility of the films although they reduce the optical transmittance of natural BMF films. The optical transmittance, in conjunction with Young's modulus, was used to determine the optimum BMF to polymer (either PVA or PEO) ratio, that is, 70:30. The AgNWs were deposited onto the surface of the respective BMF-PVA and BMF-PEO films using a creative transfer method. An optimum AgNW loading of 0.20 mg was determined based on optical transmittance and resistivity data, in comparison to commercial ITO and FTO substrates. Overall, the films are relatively uniform and are comparable to high-quality ITO and FTO products. The flexibility of the films shows potential for industrial roll-to-roll manufacturing and good thermal stability during subsequent AgNW deposition steps that require moderate to high temperatures. The ability to fabricate BMF-polymer-AgNW films that are reproducible, displays good uniformity, and have good mechanical stability makes it a practical material to utilize for next-generation flexible optoelectronics.

## 5 | EXPERIMENTAL SECTION

### 5.1 | Materials

Absolute ethanol ( $C_2H_5OH$ ), acetone ( $C_3H_6O$ ), ammonium sulfate ( $(NH_4)_2SO_4$ ), hydrochloric acid (HCl, 32%),

nitric acid ( $HNO_3$ , 55%), potassium phosphate ( $KH_2PO_4$ ), magnesium sulfate hexahydrate ( $MgSO_4 \cdot 7H_2O$ ), sodium hydroxide (NaOH), sodium hypochlorite (NaClO), sucrose ( $C_{12}H_{22}O_{11}$ ) and sulfuric acid (98%,  $H_2SO_4$ ) were obtained from Sigma Aldrich (South Africa). Ethylene glycol, polyethylene oxide ( $(C_{2n}H_{4n+2}O_{n+1})$ , average  $M_w$  of 200,000), polyvinyl alcohol ( $(C_2H_4O)_x$ , average  $M_w$  of 22,000), polyvinylpyrrolidone (average  $M_w$  of 45,000), silver nitrate ( $AgNO_3$ ) and cellulose membrane dialysis tubing (flat width 43 mm) were purchased from Merck and used as received. Mixed cellulose ester (MCE) membrane filters (47 mm  $\varnothing \times 0.4 \mu m$  pore size) were purchased from DLD Scientific. Indium tin oxide (ITO) glass substrates (56  $\times$  56  $\times$  1.1 mm; transparency >84%; resistance 15  $\Omega/sq$ ) were purchased from Luminescence Tech. Corp and fluorine-doped tin oxide (FTO) glass substrates (50  $\times$  50  $\times$  2.2 mm; transparency 80%–82%; resistance 7  $\Omega/sq$ ) were purchased from Sigma Aldrich. Ultrapure water (5.5  $\mu S m^{-1}$ ) was obtained from a Milli-Q water purification system and used during the silver nanowires synthesis. Kombucha tea (Patricia's Organic Kombucha Tea), green tea (Five Roses), brown sugar (Hulets), silicon molds and PCB heat transfer paper were purchased from South African commercial retailers. The API 20E test kit and additional reagents (TDA, James', VP1 and VP2 solutions) were obtained from bioMérieux (South Africa) for the microbial identification studies.

### 5.2 | Instrumentation

For film fabrication, an overhead IKA digital stirrer (Thomas Scientific, United States) and pneumatic, 12  $\times$  12 cm heat press FL-HP 1015 (M.C Thompson (Pty) Ltd, South Africa) were used. Ultraviolet/visible (UV/vis) absorption and transmission spectra were recorded on a Perkin Elmer Lambda 35 spectrophotometer (Japan) equipped with an integrating sphere. UV/vis spectra were collected in the range between 300 and 900 nm and collated on UV Win Lab software. Fourier transform infrared (FT-IR) spectra were obtained using a Perkin-Elmer Spectrum 100 FT-IR Spectrometer (United States) with a diamond crystal ATR accessory within the 4000–400  $cm^{-1}$  range. TEM images were obtained using a JEOL JEM 1010 microscope (Japan) designed with an objective lens pole piece. Digital images were captured using a 2 k  $\times$  2 k AMT CCD camera at an acceleration voltage of 100 kV, and images were processed using Olympus Soft Imaging Solutions. The BC microfibers were dispersed in ddH<sub>2</sub>O and subjected to sonication and negative staining using uranyl acetate before TEM imaging. Particle and fiber dimensions were determined using ImageJ Software by the National Institute of Health.

Field emission gun scanning electron microscope (FEG-SEM) images and energy-dispersive X-ray (EDX) graphs were obtained using a Zeiss Ultra Plus scanning electron microscope equipped with a field emission gun (Germany). All samples were triple gold coated and fixed onto aluminum stubs using carbon tape adhesive. SEM images were taken under high-vacuum conditions at an acceleration voltage of 20.00 kV. Due to the sensitive nature of the BC film toward the field emission gun, SEM images for the BC films were captured at an acceleration voltage of 5.00 kV. EDX measurements and element mapping were acquired through the linked Oxford X-Max detector with an 18-mm spare window and processed using AZtec Software by Oxford Instruments. XRD was carried out using a Bruker, AXS D8 Advance X-ray diffractometer (Germany), using a copper (Cu) source with  $K_{\alpha 1} = 0.154$  nm operating at 40 kV and 40 mA. The BC composite films were fixed flush onto the metal holder while the AgNWs were compacted into the central cavity of the metal holder. The diffractograms were processed using Origin software. A DMA Q-800 analyzer (TA Instruments, United States) was used to obtain stress-strain curves for the films. Thermogravimetric analysis of the films was measured using a Perkin Elmer Simultaneous Thermal Analyzer (STA 6000) (United States) under  $N_2$  conditions, heating to a maximum of 850°C at a rate of 10°C min<sup>-1</sup>. The conductive films' sheet resistance was measured using an in-house designed apparatus that measures the films' resistance over a surface area of 1 cm<sup>2</sup> at 25°C. The apparatus is further described in Figure S16.<sup>63</sup> Ultrapure water was obtained from a Milli-Q water purification system (France).

## 5.3 | Experimental details

### 5.3.1 | Biosynthesis of BC

#### *Cultivating SCOBY*

Kombucha tea (1000 mL) with small amounts of SCOBY visibly present was purchased from a local health shop and was transferred into a large, sterilized glass container. Green tea brewed in boiling water (1000 mL) was cooled to room temperature before adding to the Kombucha tea. Commercial brown sugar (~80 g) was added to the tea mixture and stirred until complete dissolution. The mixture was then equally divided into four 500 mL sterilized, wide neck glass jars. The jars were sealed using semi-permeable cloths and incubated in a darkened room at room temperature. After 3 days, visible growth of the SCOBY as a thin, gelatinous layer was observed at the liquid and air interface. After 2 weeks, the SCOBY was

removed from the Kombucha tea medium and used for the biological growth of BC.

#### *Biological growth of BC*

A HS medium for BC growth was prepared from literature procedures.<sup>71</sup> Briefly, sucrose (50.0 g), ammonium sulfate (5.0 g), yeast extract (5.0 g), potassium phosphate (3.0 g), and magnesium sulfate heptahydrate (0.05 g) was dissolved in boiling water (1000 mL). Once cooled to room temperature, the HS medium was transferred with the SCOBY to a sterilized plastic tray. It was covered with a semi-permeable material and incubated in a darkened room at room temperature (aerobic conditions). After 2–3 weeks, the BC pellicle was removed and washed thoroughly with water. The BC pellicle was treated with 0.25 M NaOH solution for 24 h and then bleached for 24 h with a NaClO solution (15 wt%). The bleached BC pellicle was washed with water and stored in double distilled water with a maintained pH of ~7.

#### *Hydrolysis of BC to BMF*

The BC pellicle was cut into smaller pieces and liquidized using a commercial household blender. The liquidized BC was vacuum-filtered overnight to remove excess water and retained a pulp-like consistency. The BC pulp was added to a beaker and hydrolyzed with stirring at 55°C using 60 wt% H<sub>2</sub>SO<sub>4</sub> (in a ratio of 0.5 g BC pulp to 1 mL H<sub>2</sub>SO<sub>4</sub>). After 5 h, the hydrolysis reaction was stopped by diluting the reaction 10-fold of cold deionized water (diH<sub>2</sub>O) to the acid mixture. The hydrolyzed BC was centrifuged numerous times to reduce the H<sub>2</sub>SO<sub>4</sub> content before dialysis treatment. The acid-BC mixture was poured and secured into MCE dialysis socks and left to dialyze in a reservoir of diH<sub>2</sub>O with stirring. The pH of the diH<sub>2</sub>O was frequently monitored and replenished accordingly until a pH of 6 was obtained. The dialyzed BC was stored in glass jars until confirmed as microfibrils (BMF) using electron microscopy analysis.

### 5.3.2 | Fabrication of BMF-polymer composite films

A PVA solution (5 wt%) was prepared by dissolving PVA (2.5 g) in ddH<sub>2</sub>O (50 mL), and stirring under reflux conditions. The dialyzed BMF was concentrated into a 10 mg mL<sup>-1</sup> stock solution and stirred continuously using an overhead stirrer to create a well-dispersed BMF suspension. Composition optimization studies were conducted by varying the BMF to polymer ratios to create the films. The appropriate volumes of BMF and PVA were combined into centrifuge tubes that were submerged in a beaker of water and exposed to ultrasonication for 10 min to obtain a

homogenous mixture of the BMF and PVA. The homogenous mixtures were then set into molds and left to air-dry overnight. The same procedure was followed to prepare the BMF-PEO composite films. The ratios used to prepare the BMF-polymer composite films are shown in Table S7.

### 5.3.3 | Synthesis of silver nanowires and conductive film fabrication

#### *Silver nanowires*

The AgNWs were synthesized via a polyol method, based on literature.<sup>72</sup> An AgNO<sub>3</sub> solution (0.1 M, 50 mL) and PVP solution (0.54 M, 50 mL) with trace amounts of HCl (1.8 wt%) and HNO<sub>3</sub> (3.2 wt%) were made up in EG. The AgNO<sub>3</sub> solution was preheated to 110°C with stirring for 30 min. The PVP solution was then injected dropwise into the preheated solution using an automated syringe pump. A temperature of 140°C was maintained with stirring for 1 h, eventually forming a wispy gray solution. The solution was left to reach room temperature, and an excess of acetone and ethanol was added. The AgNW solution was subsequently sonicated and centrifuged several times to remove the viscous PVP and ethylene glycol remnants. The AgNWs were dispersed and stored in absolute EtOH.

#### *Conductive BMF-polymer composite films*

An AgNW stock solution of ~1 mg mL<sup>-1</sup> in EtOH was prepared. The stock solution was sonicated in a water bath at a low frequency for 30 min to obtain a well-dispersed suspension. The suspension was then diluted with ddH<sub>2</sub>O, according to Table S8, to obtain well-dispersed AgNW suspensions.

Using a membrane filtration system, the respective dispersed AgNW solutions were passed through an MCE membrane filter (0.4 μm pore size). The AgNWs were collected on the surface of the MCE membrane filter. Once air-dried, the MCE membrane filter was placed AgNW side down onto a piece of PCB heat transfer paper. The MCE membrane filter and PCB heat transfer paper were mechanically pressed using a pneumatic heat press for 60 s at 90°C. The MCE membrane filter was gently peeled off, leaving behind the conductive network AgNWs on the surface of the PCB heat transfer paper.

The PCB heat transfer paper was then placed with the AgNW side down onto the respective optimized BMF-polymer film (i.e., films C or C1) and was mechanically pressed with the pneumatic heat press for 15 s at 150°C. The PCB heat transfer paper was gently peeled off, leaving behind the transferred conductive network AgNWs on the surface of the composite film. This process was repeated for all the AgNWs loadings, see Table S9.

## AUTHOR CONTRIBUTIONS

**Denisha Gounden:** Conceptualization (equal); data curation (lead); formal analysis (lead); methodology (equal); writing – original draft (lead). **Michael N. Pillay:** Conceptualization (supporting); data curation (supporting); formal analysis (supporting); writing – original draft (supporting). **Vashen Moodley:** Conceptualization (supporting); data curation (supporting); formal analysis (supporting). **Nolwazi Nombona:** Conceptualization (equal); funding acquisition (equal); methodology (equal); supervision (equal); writing – review and editing (equal). **Werner van Zyl:** Conceptualization (lead); funding acquisition (lead); project administration (lead); supervision (lead); writing – review and editing (lead).

## ACKNOWLEDGMENTS

This work was financially supported by the National Research Foundation (Grant number: 108424) and the University of KwaZulu-Natal (UKZN).

## CONFLICT OF INTEREST STATEMENT

The authors declare no competing financial interests or interactions that could have appeared to influence the work reported in this paper.

## DATA AVAILABILITY STATEMENT

The data that support the findings of this study are available in the supplementary material of this article.


## ORCID

Denisha Gounden  <https://orcid.org/0000-0001-5497-2153>

Michael N. Pillay  <https://orcid.org/0000-0002-7799-5857>

Vashen Moodley  <https://orcid.org/0000-0002-8851-8087>

Nolwazi Nombona  <https://orcid.org/0000-0002-9946-2568>

Werner E. van Zyl  <https://orcid.org/0000-0002-2012-8584>

## REFERENCES

- [1] J. F. Wager, M. M. Valencia, J. P. Bender, B. J. Norris, H. Q. Chiang, D. Hong, L. N. Norris, T. V. Harman, S. Park, J. T. Anderson, C.-H. Park, D. A. Keszler, J. Tate, H. Yanagi, M. F. Price, R. L. Hoffman, *Proc. SPIE* **2003**, 5080. <https://doi.org/10.1117/12.500876>
- [2] J. F. Wager, D. A. Keszler, R. E. Presley, *Transparent Electronics*, Springer US, New York **2008**. <https://doi.org/10.1007/978-0-387-72342-6>
- [3] Y.-H. Ha, N. Nikolov, S. K. Pollack, J. Mastrangelo, B. D. Martin, R. Shashidhar, *Adv. Funct. Mater.* **2004**, *14*, 615.
- [4] H. Yan, T. Jo, H. Okuzaki, *Polym. J.* **2009**, *41*, 1028.
- [5] N. Marinova, S. Valero, J. L. Delgado, *J. Colloid Interface Sci.* **2017**, *488*, 373.

- [6] D. Angmo, F. C. Krebs, *J. Appl. Polym. Sci.* **2013**, *129*, 1.
- [7] D. Angmo, N. Espinosa, F. Krebs, in *Low-Cost Nanomaterials* (Eds: Z. Lin, J. Wang), Springer London, London **2014**, p. 189. [https://doi.org/10.1007/978-1-4471-6473-9\\_8](https://doi.org/10.1007/978-1-4471-6473-9_8)
- [8] E. N. Dattoli, W. Lu, *MRS Bull.* **2011**, *36*, 782.
- [9] W. Cao, J. Li, H. Chen, J. Xue, *J. Photonics Energy* **2014**, *4*, 1.
- [10] H. Zhu, Z. Fang, C. Preston, Y. Li, L. Hu, *Energy Environ. Sci.* **2014**, *7*, 269.
- [11] H. Yano, J. Sugiyama, A. N. Nakagaito, M. Nogi, T. Matsuura, M. Hikita, K. Handa, *Adv. Mater.* **2005**, *17*, 153.
- [12] M. Nogi, H. Yano, *Adv. Mater.* **2008**, *1849*, 20.
- [13] D. Klemm, F. Kramer, S. Moritz, T. Lindström, M. Ankerfors, D. Gray, A. Dorris, *Angew. Chem. Int. Ed.* **2011**, *50*, 5438.
- [14] R. E. Cannon, S. M. Anderson, *Crit. Rev. Microbiol.* **1991**, *17*, 435.
- [15] D. Klemm, B. Heublein, H. Fink, A. Bohn, *Angew. Chem. Int. Ed.* **2005**, *44*, 3358.
- [16] J. George, S. N. Sabapathi, *Nanotechnol. Sci. Appl.* **2015**, *8*, 45.
- [17] R. W. Gerber, D. N. Leonard, S. Franzen, *Thin Solid Films* **2009**, *517*, 6803.
- [18] G. Calogero, P. Calandra, A. Irrera, A. Sinopoli, I. Citro, G. Di Marco, *Energy Environ. Sci.* **2011**, *4*, 1838.
- [19] Y. Li, Y. Wu, B. S. Ong, *J. Am. Chem. Soc.* **2005**, *127*, 3266.
- [20] K. Balantrapu, D. V. Goia, *J. Mater. Res.* **2009**, *24*, 2828.
- [21] H.-W. Tien, Y.-L. Huang, S.-Y. Yang, J.-Y. Wang, C.-C. M. Ma, *Carbon N. Y.* **2011**, *49*, 1550.
- [22] I. E. Stewart, M. J. Kim, B. J. Wiley, *ACS Appl. Mater. Interfaces* **2017**, *1870*, 9.
- [23] Y. Atwa, N. Maheshwari, I. A. Goldthorpe, *J. Mater. Chem. C* **2015**, *3*, 3908.
- [24] R. Jayabalan, R. V. Malbaša, E. S. Lončar, J. S. Vitas, M. Sathishkumar, *Compr. Rev. Food Sci. Food Saf.* **2014**, *13*, 538.
- [25] S. A. Villarreal-Soto, S. Beaufort, J. Bouajila, J.-P. Souchard, P. Taillandier, *J. Food Sci.* **2018**, *83*, 580.
- [26] C. Dufresne, E. Farnworth, *Food Res. Int.* **2000**, *33*, 409.
- [27] S.-P. Lin, I. Loira Calvar, J. M. Catchmark, J.-R. Liu, A. Demirci, K.-C. Cheng, *Cellulose* **2013**, *20*, 2191.
- [28] M. L. Sanyang, M. Jadwaid, F. Mohammad, M. S. Salit, N. Saba, in *Nanocellulose and Nanohydrogel Matrices: Biotechnological and Biomedical Applications* (Eds: M. Jawaid, F. Mohammad), Wiley, Germany **2017**, p. 55. <https://doi.org/10.1002/9783527803835>
- [29] Y. Nishiyama, G. P. Johnson, A. D. French, V. T. Forsyth, P. Langan, *Biomacromolecules* **2008**, *9*, 3133.
- [30] W. Ouarhim, N. Zari, R. Bouhfid, A. El Kacem Qaiss, in *Fibre-Reinforced Composites and Hybrid Composites*. Woodhead Publishing Series in Composites Science and Engineering (Eds: M. Jawaid, M. Thariq, B. Saba), Woodhead Publishing, Sawston, UK **2019**, p. 43. <https://doi.org/10.1016/B978-0-08-102292-4.00003-5>
- [31] H. Suryanto, T. A. Sutrisno, M. Muhajir, N. Zakia, U. Yanuhar, *MATEC Web Conf.* **2018**, *204*, 05015. <https://doi.org/10.1051/mateconf/201820405015>
- [32] Y. Habibi, L. A. Lucia, O. J. Rojas, *Chem. Rev.* **2010**, *110*, 3479.
- [33] B. G. Rånby, *Discuss. Faraday Soc.* **1951**, *11*, 158.
- [34] T. Jayaramudu, H.-U. Ko, L. Zhai, Y. Li, J. Kim, *Soft Mater.* **2017**, *15*, 64.
- [35] M. Kazemi Pilehrood, M. Dilamian, M. Mirian, H. Sadeghi-Aliabadi, L. Maleknia, P. Nousiainen, A. Harlin, *Biomed. Res. Int* **2014**, *2014*, 438065.
- [36] J. H. Kim, J. Y. Kim, Y. M. Lee, K. Y. Kim, *J. Appl. Polym. Sci.* **1992**, *45*, 1711.
- [37] Y. M. Lee, S. H. Kimt, S. J. Kimt, *Polymer* **1996**, *37*, 5897.
- [38] G. Attia, M. F. H. A. El-Kader, *Int. J. Electrochem. Sci.* **2013**, *8*, 5672.
- [39] R. Ricciardi, F. Auriemma, C. De Rosa, F. Lauprêtre, *Macromolecules* **1921**, *2004*, 37.
- [40] G. B. Hadjichristov, Y. G. Marinov, A. G. Petrov, H. K. Koduru, N. Scaramuzza, *J. Phys. Conf. Ser.* **2019**, *1186*, 12020.
- [41] G. Zardalidis, J. Mars, J. Allgaier, M. Mezger, D. Richter, G. Floudas, *Soft Matter* **2016**, *12*, 8124.
- [42] A. Arya, A. L. Sharma, *J. Phys. D: Appl. Phys.* **2017**, *50*, 443002.
- [43] H. K. Koduru, L. Marino, F. Scarpelli, A. G. Petrov, Y. G. Marinov, G. B. Hadjichristov, M. T. Iliev, N. Scaramuzza, *Curr. Appl. Phys.* **2017**, *17*, 1518.
- [44] F. E. Bailey, J. V. Koleske, in *Poly(Ethylene Oxide)*, 1st ed. (Eds: F. E. Bailey, J. V. Koleske), Academic Press, Cambridge, Massachusetts **1976**, p. 105. <https://doi.org/10.1016/B978-0-12-073250-0.50010-6>
- [45] H. Cheng, C. Zhu, B. Huang, M. Lu, Y. Yang, *Electrochim. Acta* **2007**, *52*, 5789.
- [46] H. Gupta, L. B. Shalu, V. K. Singh, S. K. Chaurasia, R. K. Singh, *RSC Adv.* **2016**, *6*, 87878.
- [47] A. Azli, N. S. Manan, M. F. Kadir, *Adv. Mater. Sci. Eng.* **2015**, *2015*, 145735.
- [48] L. E. Millon, W. K. Wan, *J. Biomed. Mater. Res. B. Appl. Biomater.* **2006**, *79*, 245.
- [49] M. F. Ashby Ed., *Materials and the Environment*, 2nd ed., Butterworth-Heinemann, Boston **2013**, p. 459. <https://doi.org/10.1016/B978-0-12-385971-6.00015-4>
- [50] Sonal, A. Sharma, S. Aggarwal, *J. Non Cryst. Solids* **2018**, *485*, 57.
- [51] D. A. Schaeffer, G. Polizos, D. B. Smith, D. F. Lee, S. R. Hunter, P. G. Datskos, *Nanotechnology* **2015**, *26*, 55602.
- [52] J. Lucas, *Curr. Opin. Solid State Mater. Sci.* **1999**, *4*, 181.
- [53] S. Hemmati, M. T. Harris, D. P. Barkey, *J. Nanomater.* **2020**, *2020*, 9341983.
- [54] J. Tauc, *Mater. Res. Bull.* **1968**, *3*, 37.
- [55] E. A. Davis, N. F. Mott, *Philos. Mag. A J. Theor. Exp. Appl. Phys.* **1970**, *22*, 903.
- [56] M. Thirumoorthi, J. T. J. Prakash, *J. Asian Ceram. Soc.* **2016**, *4*, 124.
- [57] M. S. Farhan, E. Zalnezhad, A. R. Bushroa, A. A. D. Sarhan, *Int. J. Precis. Eng. Manuf.* **2013**, *14*, 1465.
- [58] Z. Yu, I. R. Perera, T. Daeneke, S. Makuta, Y. Tachibana, J. J. Jasieniak, A. Mishra, P. Bäuerle, L. Spiccia, U. Bach, *NPG Asia Mater.* **2016**, *8*, e305.
- [59] E. Elangovan, K. Ramamurthi, *Thin Solid Films* **2005**, *476*, 231.
- [60] Z. Y. Banyamin, P. J. Kelly, G. West, J. Boardman, *Coatings* **2014**, *4*, 732.
- [61] H. Kim, R. C. Y. Auyeung, A. Piqué, *Thin Solid Films* **2008**, *516*, 5052.
- [62] J. Xu, W. Liu, H. Liu, Y. Hu, *Front. Chem. Eng. China* **2007**, *1*, 221.
- [63] N. Nirmal, M. N. Pillay, M. Mariola, F. Petruccione, W. E. van Zyl, *RSC Adv.* **2020**, *10*, 27585.
- [64] Z. Sun, C. Cao, Q. Cai, X. Song, *Sci. China Technol. Sci.* **2010**, *1893*, 53.
- [65] L. H. Lalasari, T. Arini, L. Andriyah, F. Firdiyono, A. H. Yuwono, *AIP Conf. Proc* **2018**, *1964*, 20001.

- [66] Y. Jia, C. Chen, D. Jia, S. Li, S. Ji, C. Ye, *ACS Appl. Mater. Interfaces* **2016**, 8, 9865.
- [67] J. Park, J. Moon, *Langmuir* **2006**, 22, 3506.
- [68] L. W. Schwartz, R. V. Roy, R. R. Eley, S. Petrash, *J. Colloid Interface Sci.* **2001**, 234, 363.
- [69] D. Soltman, V. Subramanian, *Langmuir* **2008**, 24, 2224.
- [70] M. Layani, M. Gruchko, O. Milo, I. Balberg, D. Azulay, S. Magdassi, *ACS Nano* **2009**, 3, 3537.
- [71] S. Hestrin, M. Schramm, *Biochem. J.* **1954**, 58, 345.
- [72] H. Guo, G. Xing, Z. Yang, *Proceedings of the 2015 International Symposium on Material, Energy and Environment Engineering*, Atlantis Press, Amsterdam, The Netherlands **2015**, p. 39. <https://doi.org/10.2991/ism3e-15.2015.11>

## SUPPORTING INFORMATION

Additional supporting information can be found online in the Supporting Information section at the end of this article.

**How to cite this article:** D. Gounden, M. N. Pillay, V. Moodley, N. Nombona, W. E. van Zyl, *J. Appl. Polym. Sci.* **2023**, 140(30), e54090. <https://doi.org/10.1002/app.54090>